Indirect assessment of concrete resistance from FE model updating and Young's modulus estimation of a multi-span PSC viaduct: Experimental tests and validation

Indirect assessment of concrete resistance from FE model updating and Young's modulus estimation of a multi-span PSC viaduct: experimental tests and validation

Angelo Aloisio[a], Dag Pasquale Pasca[b], Luca Di Battista[a], Marco Martino Rosso[c,*], Raffaele Cucuzza[c], Giuseppe Carlo Marano[c], Rocco Alaggio[a]

[a]*Civil Environmental and Architectural Engineering Department, Università degli Studi dell'Aquila, via Giovanni Gronchi n.18, L'Aquila, 67100, Italy*
[b]*Norsk Treteknisk Institutt, Børrestuveien 3, Oslo, 0373, Norway*
[c]*Politecnico di Torino, DISEG, Dipartimento di Ingegneria Strutturale, Edile e Geotecnica, Corso Duca Degli Abruzzi, 24, Turin, 10128, Italy*

Abstract

The paper discusses the possibility of reliably estimating the concrete resistance based on Young's modulus assessed from FE model updating using ambient vibration data. The procedure is applied to the FE model updating of a multi-span prestressed concrete bridge in Corvara (Italy). The bridge consists of seven spans, each made of seven prestressed concrete girders and a concrete deck. The operational modal analysis of the seven spans leads to estimating Young's moduli of the deck and the girders. The FE model's sensitivity analysis shows the modal parameters' dependence to the Young moduli of the deck and the girders, proving that the detected modes are differently affected by the two modelling parameters. In a second step, the authors estimate the concrete resistance using a well-acknowledged empirical correlation between the Young moduli from FE model updating and the concrete resistance. Finally, the concrete resistance and its uncertainty, obtained by propagating the modelling error from the objective function to the concrete resistance, is compared to the concrete resistance assessed from destructive tests on concrete samples extracted from the bridge. The paper confronts the values of concrete resistance estimated from a non-destructive and a destructive method. The indirect method based on the tuning of the FE model yields a good matching in terms of estimated parameters. However, the variance from concrete samples is higher than that obtained from the indirect method. The authors discuss the causes of this discrepancy and highlight the pros and cons of the presented indirect method for estimating the material properties from ambient vibration data.

*Corresponding author.
Email address: marco.rosso@polito.it (Marco Martino Rosso)

Keywords: structural health monitoring, operational modal analysis, model updating, Young's modulus, concrete strength

1. Introduction

The ageing of concrete structures urges the need for methods to assess the material properties from experimental data [1, 2]. The last decades saw the spreading of dynamics-based practices to determine the health of structures [3, 4], damage detection strategies [5, 6], and in particular the state of concrete [7, 8, 9]. Most of them focus on the issue of damage detection and localization and present challenging methods to estimate the structural damage using vibration data [10, 11, 12, 13]. In concrete structures, Young's modulus can be a global representative of the health of the whole structural system [14, 15]. It is sensitive to several ageing factors such as e.g. micro-cracking phenomena or the conservation state of the cementitious paste, behaving as a homogenized parameter of several decaying agents [16, 17]. Therefore, the estimate of Young's modulus bestows a significant insight into the conservation state of a concrete structure [18]. The actual goal of structural assessment is structural reliability, thus the estimation of Young's modulus is an intermediate fundamental step [19], which is related to the material resistance. The scientific literature and the National standards present several empirical correlations between Young's modulus and the compressive strength of concrete [20]. In this paper, the authors discuss the possibility of indirectly estimating the concrete resistance from Young's modulus, regarded as an indirect estimator of the ultimate capacity [21] and assessing it from vibration data. There are several research papers [22, 23, 24] and standards for the estimation of Young's modulus from the vibration of concrete specimens. Specifically, there are normalized methods for assessing the elastic properties of a material using the recorded vibrations of specimens, such as the American Society for Testing and Materials [25] or the Deutscher Ausschaussfür Stahlbeton [26]. Additionally, it is common in civil engineering to estimate Young's modulus from FE model updating based on the outcomes of operational modal analysis (OMA) [27, 28], by calibrating a set of the stiffness parameters based on the experimental operational response. Furthermore, Young's moduli of concrete may return an indirect estimate of the concrete strength using acknowledged correlations. However, there are a few equations showing relationships between those two parameters [29]. Besides, the

value of Young's modulus of concrete depends on many other factors such as moisture, the percentage of aggregate volume, density, and aggregate type. The discussed procedure based on FE model updating can also lead to assessing the variance of the concrete resistance. The variance of the objective function, known from the optimization problem, is propagated to Young's moduli and then to the concrete resistance to assess the expected tolerances of the estimates. Several authors [30, 31, 32, 33, 34, 35] distinguish multiple types of uncertainties, which can be at least classified into two sources: the uncertainty of the prediction model and that related to the experimental data. In this research, the authors evaluate the tolerances of the estimates, considered, according to [36], among the model uncertainties.
The values of the concrete resistances, indirectly estimated from the FE model updating [37, 30], are finally compared to the ones directly estimated from concrete samples extracted from the bridge girders. The authors compare and discuss the results by highlighting the pros and cons of these indirect properties estimations from ambient vibration tests. The paper has the following structure: the first part (section 2) outlines the indirect method for estimating the resistance of concrete from ambient vibration data. The second part (section 3) presents the case study and the experimental tests. Section 4 presents the results from the FE model updating, while the last section compares the direct and indirect methods for estimating concrete resistance.

2. Indirect estimate of the material resistance from FE model updating using ambient vibration data

Deterministic model updating leads to an optimal set of model parameters $\hat{\boldsymbol{\theta}}_M$ that minimizes the misfit between experimental data, denoted as $\boldsymbol{d}$, and model predictions denoted as $\boldsymbol{G}_M(\boldsymbol{\theta}_M)$. This discrepancy is represented by the so-called misfit or cost function $\mathcal{F}$, so that the model updating problem is equivalent to the following optimization problem [36, 38]:

$$\hat{\boldsymbol{\theta}}_M = \arg\min_{\boldsymbol{\theta}_M} \mathcal{F}\left(\boldsymbol{G}_M(\boldsymbol{\theta}_M) - \boldsymbol{d}\right) | \boldsymbol{\theta}_M \in \mathcal{D} \subseteq \mathbb{R}^{N_{\boldsymbol{\theta}_M}} \tag{1}$$

The experimental data $\boldsymbol{d}$ used for damage assessment through FE model updating most often consist of measurements obtained during dynamic vibration experiments, where a structure is equipped with a set of measurement

sensors (e.g. accelerometers, strain gauges, fibre-optic sensors) which register the system's response due to some dynamic excitation. In structural dynamics, the most used parameters for model updating are the modal parameters, generally estimated from OMA. In civil structures, the modelling parameters ($\hat{\boldsymbol{\theta}}_M$) are generally the geometric and material features, which directly affect the modal parameters. The geometric features are mainly known from a direct survey and assumed as given data. Therefore, model updating generally comes down to only assessing the stiffness parameters of a FE model. The goal of the FE element model updating is to obtain a numerical or mathematical model that can simulate the structural behaviour for analysis, prediction, and design purposes. In civil engineering practice, FE models have primarily been used to analyze structural performance under different limit states. However, the use of FE models to assess the structural performance under ultimate limit states entails plausible assumptions about material resistance. Specifically, while the stiffness parameters can be directly calibrated using ambient vibration data, the material resistances necessary for ultimate limit state assessments are generally assumed or estimated from additional experimental tests, generally destructive tests based on the extraction of structural samples. The FE model updating using the modal parameters can estimate the stiffness parameters, not the strength of the material, which is generally assessed from additional experimental tests. Still, the stiffness features are generally related to the resistance, and several standards propose empirical correlations between the stiffness and resistance of the materials. Expressly, there are acknowledged algebraic relationships between Young's modulus and compressive resistance of concrete. So far, a few scholars have attempted to estimate the material properties from the stiffness parameters estimated from FE model updating based on ambient vibration data [39]. This research presents a case study where the indirect estimation of the concrete resistance from Young's modulus assessed from FE model updating is compared to the resistance directly estimated from concrete samples. The goal is to discuss the applicability of an indirect approach for assessing the compressive strength of concrete in practical applications, where data from concrete samples are available. Four steps are the base of the proposed method for the indirect estimation of the concrete resistance from ambient vibration data.

1. **Step 1-Preliminary FE model**. The development of a FE model of the structure is the preliminary task. The modal analysis of the

numerical model, obtained by adopting first-attempt estimates of the parameters, may assist the scholar in the optimum sensor placement of the measurement devices (accelerometers, velocimeters, strain gauges, e.g.).

2. **Step 2-Experimental tests**. The estimation of the experimental modal parameters from ambient vibration data is the second step. The scientific literature of the last two decades bestows diverse and efficient techniques for extracting modal features [40]. The scholar can obtain the modal parameters from single experimental campaigns. Still, the increasing interest in permanent monitoring systems may allow a more in-depth investigation of the structural response by tracking the estimated parameters over time [41, 42].
3. **Step 3-FE model updating**. The optimization of the FE model using the experimental modal parameters is the third step. Model updating problems are inverse problems since the objective is to obtain the parameters that produce a given output. Deterministic model updating aims to find the optimal parameters associated with the best fit between the model output and the observed data. The optimal parameters are generally obtained from a constrained optimization problem, where the objective is to minimize the discrepancy between computed and measured data. In many cases, however, this optimization problem is prone to ill-posedness and ill-conditioning, meaning that the existence, uniqueness and stability of a solution of the inverse problem cannot be guaranteed. Since the experimental modal parameters from OMA are unscaled to the mass matrix, the mass and the stiffness matrices cannot be both unknowns. However, the geometry of the structures and the specific weight of the materials can be estimated with sufficient detail. Therefore, the mass matrix can be assumed as known, and the optimization may focus on the more uncertain structural features: the boundary restraints and the elastic parameters. The variance matrix of the optimum parameters $\boldsymbol{\Sigma}_{\hat{\boldsymbol{\theta}}_{\boldsymbol{M}}}$ can be estimated by propagating the variance of minimum value of the objective function using a first-order approximation of the objective function by the minimum point.

$$\boldsymbol{\Sigma}_{\hat{\boldsymbol{\theta}}_{\boldsymbol{M}}} = \left(\boldsymbol{J}_{\hat{\boldsymbol{\theta}}_M,\mathcal{F}}\right)^{\dagger} \sigma_{\mathcal{F}}^2 \left(\boldsymbol{J}_{\hat{\boldsymbol{\theta}}_M,\mathcal{F}}^T\right)^{\dagger} \tag{2}$$

where $\sigma_{\mathcal{F}}^2$ is the variance of the objective function in the minimum point, $\boldsymbol{J}_{\hat{\boldsymbol{\theta}}_M,\mathcal{F}} = \frac{\partial \mathcal{F}}{\partial \boldsymbol{\theta}^M} | \boldsymbol{\theta}_M = \hat{\boldsymbol{\theta}}_M$ is the Jacobian matrix of the objective

function evaluated by the optimum point, while ^{T} and † denote the transpose matrix and the pseudo-inverse operator, respectively.

4. **Step 4-Estimation of the material resistance**. The empirical relationship between the resistance $\boldsymbol{R}$ and the modelling parameters can be written as follows:

$$\boldsymbol{R} = \boldsymbol{R}(\boldsymbol{\theta}_M) \tag{3}$$

The estimates of the material resistance ($\hat{\boldsymbol{R}}$) can be obtained by evaluating Eq.(3) in $\boldsymbol{\theta}_M = \hat{\boldsymbol{\theta}}_M$. The covariance matrix of the estimated resistance ($\boldsymbol{\Sigma}_{\hat{\boldsymbol{R}}}$) can be obtained from the first-order approximation of Eq.(3):

$$\boldsymbol{\Sigma}_{\hat{\boldsymbol{R}}} = \left(\boldsymbol{J}_{\hat{\boldsymbol{\theta}}_M,\boldsymbol{R}}\right) \boldsymbol{\Sigma}_{\hat{\boldsymbol{\theta}}_M} \left(\boldsymbol{J}^T_{\hat{\boldsymbol{\theta}}_M,\boldsymbol{R}}\right) \tag{4}$$

where $\boldsymbol{J}_{\hat{\boldsymbol{\theta}}_M,\boldsymbol{R}} = \frac{\partial \boldsymbol{R}}{\partial \boldsymbol{\theta}_M} | \boldsymbol{\theta}_M = \hat{\boldsymbol{\theta}}_M$ is the Jacobian matrix of Eq.(3) evaluated by the optimum values of the parameters.

3. Case study: the Corvara bridge

The proposed procedure is tested on a prestressed concrete bridge in Corvara (Pescara, Italy), shown in Fig.1. The viaduct, built in 1987, has a structural scheme with a deck and girders. Each span is made up of eight juxtaposed prestressed concrete (PSC) prefabricated girders (type TAS-PN 120/46) and reinforced concrete decking. The dimensions and geometric characteristics are shown in the Tab.1.

Table 1: Dimensions of the bridge

Component	**Dimensions [m]**
Span length	20.00
Sidewalk width	0.50
Track width	7.50
Total width	8.50
Deck height	1.45

The viaduct consists of seven spans. Fig.2 depicts the longitudinal and transverse cross-section of a sample span. The authors chose the Corvara bridge for the following reason: the bridge can be considered as an average representative of the secondary viability infrastructures, which are the more overlooked and do not usually deserve the investment of a permanent monitoring system. Therefore, dynamics-based methods may benefit the assessment of structural health in the form of daily experimental campaigns.

(a) (b)

(c) (d)

Figure 1: (a) Global view of the Corvara bridge; (b)-(c) Side and bottom view of a single span; (d) Detail of the supports.

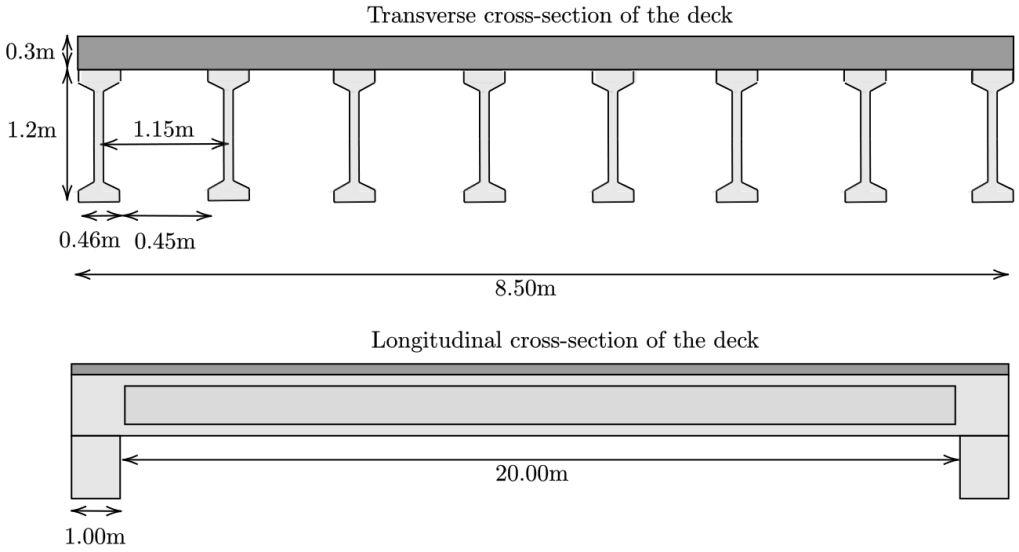

Figure 2: Transverse and longitudinal cross-section of the bridge

The bridge is likely to be in a good conservation state, despite the lack of a proper rainwater drainage system. Additionally, the deck lacks bearings: the piers support the bridge without any load transfer device.

3.1. Dynamic Identification

On 4$^{\text{th}}$ August 2020, the authors measured the response of the bridge to ambient excitation. They independently recorded the one-hour structural vibration of each span. The closing of the bridge during the experimental campaign caused a shallow level of vibration with root-mean-square value below 0.1 mg (see Fig.3).

Fig.4 details the experimental setup: ten biaxial Force-Balance accelerometers were arranged in two symmetric measurement chains, placed 1.30 m from the lateral edges. The extreme accelerometers were in correspondence of the edges of the span; the remaining accelerometers were equally spaced. A master recording unit headed each measurement chain, powered by a 12V battery. The GPS signal synchronized the two independent chains, and the data were sampled at 200 Hz.

The experimental modal parameters are obtained from the processing of the experimental data using the Enhanced Frequency Domain Decomposition (EFDD) [43] and the Stochastic Subspace Identification algorithm (SSI)

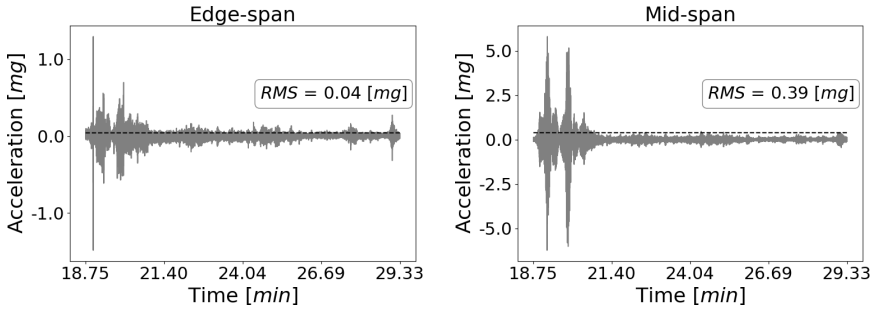

Figure 3: Sample time histories by the edge and mid-span with indication of the root-mean-squared (rms) value of the signal.

[44]. The EFDD method, which is a so-called non-parametric, frequency domain procedure, and SSI-cov, which is a parametric, time-domain procedure, are probably among the two most used techniques for OMA nowadays [3]. Two routines, written by the authors using Python programming language, were developed to extract the modal parameters according to the previously mentioned algorithms. In particular, Fig.4 (c) illustrates the dynamic identification results of SSI-cov method in terms of stabilization diagram. The actual unknown model order, shown in the vertical axis, is progressively increased and the solution poles of the identification procedure for each order are marked to the corresponding natural frequency, depicted in the horizontal axis in Hz. To summarize more information in a single graph about every potential solution, a color map has been adopted in order to show stability characteristics of every pole, by adopting the well-established stability requirements criteria respectively based on frequency, damping and modal assurance criterion (MAC) of the mode shapes [3]. The first four experimental modes have been identified by the main alignments of the stable poles. Despite the low level of excitation, the stabilization diagram returns four stable modes in the frequency range 0-20 Hz. Tab.2 report the estimated natural frequencies and damping ratios of the seven spans, while Fig.5 depicts the mode shapes associated with each of the four modes.

The very first alignment of poles in the stabilization diagram corresponds to a rigid translational mode. The authors started the counting of the modes from the first deformational at nearly 7 Hz. As noticed by [15, 45] in a different set of identical prestressed concrete girders, the first mode shapes are very alike between each other (MAC >0.99), while the values of the natural frequencies of the first modes are very scattered. Indeed, the first mode shapes

(a) (b)

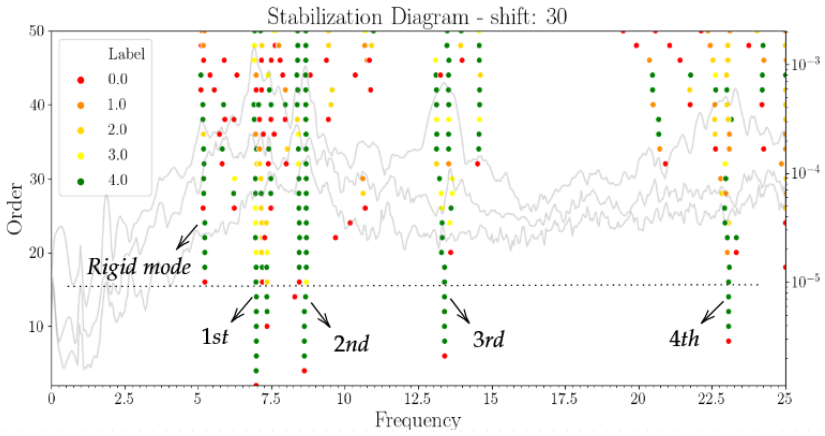

(c)

Figure 4: View of the experimental setup: (a) the master recording unit and the laptop, (b) ten biaxial Force Balance Accelerometers (c) stabilization diagram. The colours of the poles, identified by the numbers 0.0 to 4.0 in the legend indicate respectively: unstable, stable in frequency, stable in frequency and mode shape, stable in frequency and damping, stable in frequency damping and mode shape.

Table 2: Experimental natural frequencies of the detected modes of the seven spans: f_i and ξ_i indicate the natural frequency and damping ratio of the i-th mode.

Span no	f_1 [Hz]	ξ_1 [%]	f_2 [Hz]	ξ_2 [%]	f_3 [Hz]	ξ_3 [%]	f_4 [Hz]	ξ_4 [%]
1	7.38	1.58%	9.15	1.29%	14.20	1.70%	-	-
2	7.17	1.55%	8.68	1.93%	14.10	1.33%	23.53	1.22%
3	7.33	1.64%	8.87	1.12%	13.45	1.34%	-	-
4	6.98	1.13%	8.62	1.26%	13.39	1.58%	23.06	2.05%
5	6.95	1.95%	8.44	1.34%	13.42	1.58%	22.89	1.10%
6	7.15	1.81%	8.53	1.09%	14.14	1.50%	23.73	1.15%
7	7.17	1.69%	8.55	1.17%	14.60	1.42%	-	-

Table 3: FE Participating mass ratios of the four OMA identified modes for the central span: r_{mx}, r_{my}, r_{mz} are referred to the translational masses in the cartesian global coordinate system (x: longitudinal direction, y transversal direction and z vertical direction), whereas $r_{mrx}, r_{mry}, r_{mrz}$ considers the rotational masses around the global coordinate axis.

Mode no.	r_{mx} [%]	r_{my} [%]	r_{mz} [%]	r_{mrx} [%]	r_{mry} [%]	r_{mrz} [%]
1	0	0	81.00	0	0	0
2	0	8.211	0	73.00	0	0
3	0	39.00	0	3.053	0	0
4	1.407	0	0	0	61.00	0

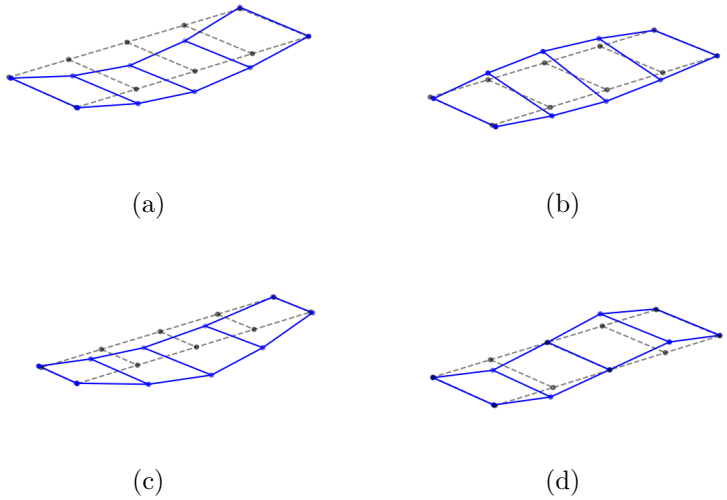

(a) (b)

(c) (d)

Figure 5: Experimental mode shapes of a sample bridge span: (a) first mode: first pure translational vertical direction; (b) second mode: first torsional; (c) third mode: translational coupled vertical and transverse directions; (d) fourth mode: second pure translational vertical direction. The dashed lines is the sensor placement geometry undeformed shape, whereas the blue solid lines represent the simplified mode shape obtained connecting in a linear way the nodes for which the mode shapes coordinates have been calculated.

resemble those of a simply supported girder, where the displacement by the supporting piers is almost zero, see Fig.5. This evidence may suggest that there is no significant difference in the boundary restraints between the seven spans. The scatter of the natural frequencies may originate from a dispersion of Young's moduli of concrete. The value of Young's modulus in concrete is quite scattered, and even a slight variation can yield notable changes in the natural frequencies. Therefore, the FE optimization aims at identifying the

diverse Young's moduli associated with each span. The second mode is the first torsional mode. Differently from [45], vertical modal component by the support is nearly zero, due to the lack of bearing devices and the low level of excitation. The excitation does not activate the mono-lateral nature of the constraint: the torsional constraint may be more alike to prevent rotation by the supports. The second mode shape may give significant pieces of information about the torsional response of the bridge deck. These structures may be considered as ribbed plates, characterized by the peculiar torsional response of the cross-section, still object of several research efforts [46]. However, this investigation is beyond the purpose of the current paper and will be the object of future studies. The considered measurement setup does not allow an unambiguous distinction between the first and the third modes. Actually, referring to the experimental mode shape illustrated in Fig.5, in OMA, only the sensors setup arrangement geometry is considered in the mode shape reconstruction and a linear interpolation is performed among the locations of the sensors. From a visualization point of view only, the user is not able to immediately distinguish the first mode from the third one. The FE element will reveal the diversity between them. Still, Fig.5 may evidence the notable role of the horizontal displacement in the third mode: differently from the first mode shape, the vertical bending is coupled with a horizontal deformation of the cross-section. The fourth mode resembles the second mode of a beam-like structure. The authors could not identify the fourth mode in all the tested spans. However, when its identification was successful, the mode shape corresponds precisely to the mode shape of the second mode of a pinned girder. Additionally, comparing the results among the spans, the natural frequencies of the second mode are more similar among themselves with respect to those of the first mode. The damping ratios span between 1.5 and 2%. These values are consistent with those found by other scholars in concrete structures in operational conditions [47]. The participating mass ratios, illustrated in Tab.3, provided a good agreement with the experimental OMA founded modes and support the aforementioned reasoning. In particular, the fourth mode is related to a rotational mass with respect to the transverse axis, evidencing a mode shape which is quite similar to the second pure translational vertical mode.

4. Model calibration

The authors developed a FE model in Sap2000, by assembling eight beam elements and a shell element with a vertical offset equal to the difference between the centre of gravity of the girders and that of the deck. Fig.6

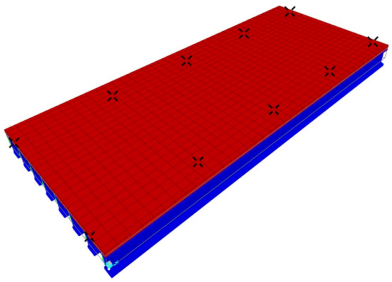

Figure 6: FE model with the marks of the positions of the accelerometers.

depicts the extruded FE model with black cross marks by the position of the accelerometers. The boundary restraints are assumed pinned-pinned. The authors estimated the optimum FE element model of each span, by minimizing the following objective function [38]:

$$\mathcal{F} = \sum_{i=1}^{M} \gamma_i \left(\frac{\omega_i^m - \omega_i^c}{\omega_i^m} \right)^2 + \beta \sum_{i=1}^{M} (1 - \mathrm{diag}(MAC(\Phi_i^m, \Phi_i^c))) \qquad (5)$$

where the superscript $(*)^m$ indicates a measured variable, the superscript $(*)^c$ a calculated variable, Φ_i is the mode shape vector, M is the number of modes, MAC is the Modal Assurance Criterion [48], while γ_i and β are weighting factors. The main challenges in finding the agreement between experimental and numerical mode shapes depended on the chosen arrangement of the accelerometers. In the adopted experimental setup, two longitudinal rows of accelerometers close to the deck edges are used. Since OMA provides modal coordinates only for the points corresponding to the locations of the sensors, the resulting mode shapes of the first and third modes may appear substantially identical for the user, see Fig.5. Thus, the scholar, as discussed in the previous section, could erroneously exchange the first mode with the third one.

4.1. Sensitivity Analysis

Before estimating the optimum values of the modelling parameters, sensitivity analysis provided a quantitative assessment of their effect of the chosen

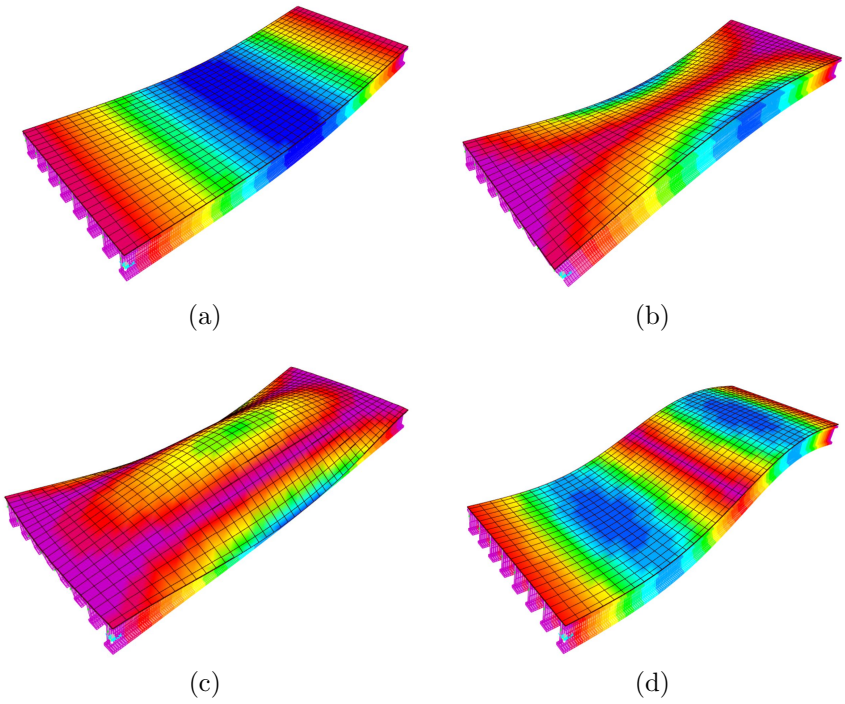

Figure 7: (a)-(d) The Finite Element mode shapes of the bridge span corresponding to the experimental ones.

objective function, in Eq.5, and the first four natural frequencies. The authors chose the Young's moduli of the girder and the deck, labelled E_b and E_d respectively, as the unknown structural parameters.
The two Young's moduli were the base of a variance-based sensitivity analysis. The analysis allowed decomposing the variance of the output (objective function, and natural frequencies) of the model into fractions which can be attributed to the chosen mechanical parameters [49]. The first step was setting the inputs sampling range (mean value in Tab.4 $\pm 30\%$) and generating the model inputs according to the Saltelli's sampling scheme [50]. These sampling range values represent the initial model parameters adopted considering the nominal values which have been expected at the time of the bridge construction, e.g. retrieved from original technical documentation. The deck was expected to be constituted by a concrete material with characteristic nominal strength of 55 MPa, whereas 30 MPa was expected to be adopted for the deck slab. Adopting e.g. the Italian code empirical rela-

tionship, it is possible to determine the initial Young's modulus value both for the beam and the deck. The variance is even taken from code provisions and propagated to also estimate the standard deviation of Young's modulus. ($N \cdot (2D + 2)$ model inputs were generated, where $N = 100$ is the number of samples, and $D = 2$ is the number of input parameters). After running

Table 4: Design values of the resistance and Young's modulus of concrete in MPa.

Structure	f_k	σ_f	E	σ_E
girder	55.00	4.88	36688.63	194.78
Deck	30.00	4.88	30588.56	297.73

all the model inputs the first-order (S_1) and total-order (S_T) sensitivity indices were calculated. S_1 and S_T measure respectively, the effect of varying a single parameter alone and the contribution to the output variance of the selected parameter including all variance caused by its interactions with the other parameters. Tab.5 lists the sensitivity indicators, where the two rows refer to E_b and E_d, respectively.

Table 5: Results of the variance-based sensitivity analysis in terms of Sobol Indicators.

Parameters	Objective Function		f_1		f_2		f_3		f_4	
	S_1	S_T	S_1	S_T	S_1	S_T	S_1	S_T	S_1	S_T
E_b	28.8%	37.0%	30.8%	29.8%	21.5%	20.5%	17.9%	17.1%	87.5%	87.1%
E_d	63.8%	72.1%	71.2%	69.5%	80.5%	79.0%	84.0%	82.6%	13.6%	12.4%

Both the objective function in Eq.5 and the first three natural frequencies are more sensitive to Young's modulus of the concrete deck. The sensitivity indexes S_1 and S_T referred to E_d span between 70% and 80%. Parallelly, the sensitivity indexes of E_b range between 30% and 20%. The similarity between S_1 and S_T proves that the two indicators are substantially uncorrelated parameters. Conversely, the natural frequency of the fourth mode is primarily affected by Young's modulus of the supporting girders. This fact is consistent with the mode shape of the fourth mode, which resembles a second mode of an equivalent beam. This mode is associated with a more significant deformation of the girders. Conversely, the second and the third modes mainly reveal the torsional deformation of the deck. The modal parameters express a marked dependence on the chosen modelling parameters, E_b and E_d. Therefore, the two Young's moduli can be chosen as unknown parameters in the FE model updating. Model updating is an inverse problem prone to ill-posedness and ill-conditioning. However, if the model updating problem

is well-posed and well-conditioned, the model uncertainties can be considered negligible, as shown in the next sections. For this purpose, the authors assumed the specific weight of concrete, which exhibits reduced variability, and the structural geometry obtained from a detailed survey. At the same time, the two Young's moduli are the sole unknowns in FE optimization.

4.2. Results

Two optimization algorithms were used to solve the global optimization problem in Eq.5, the Differential Evolution (DE) [51] and the Particle Swarm Optimization (PSO)[52]. The two algorithms were used for mutual validation of the correctness of the results. Since the outcomes of the two algorithms were nearly coincident, the authors report the sole optimum values from the DE algorithm. The relative tolerance for convergence was set equal to 0.01. Therefore, the variance of the objective function ($\sigma_{\mathcal{F}}$) is approximately $\sigma_{\mathcal{F}} \approx \mathcal{F}(\hat{\theta_M} \cdot 0.01$. The automated run of the optimization originates from the use of the SAP2000 Open Application Programming Interface (OAPI) driven by Python code. Tab.8 shows the comparison between the experimental and optimal numerical natural frequencies of the seven spans. The percentage error between each pair of values is approximately below 15%. As typical in FE model updating with modal parameters [53], the relative error increases as the model order grows. Still, the correspondence is very satisfactory and the FE model achieves a good matching with the experimental data. The MAC values of the first, second and third modes are, on average, higher than 90%. However, a lower correspondence is achieved with the third mode. This fact depends on the possible lower accuracy in estimating the mode shapes since the accelerometers were placed where the modal displacement was almost the lowest, see Fig.7(c). According to the Italian National Standards [54], the empirical correlation between Young's modulus and the compression strength of concrete can be written as:

$$E = 22000 \cdot \left(\frac{f}{10}\right)^{0.3} \tag{6}$$

where E is mean value of Young's modulus and f is the mean value of the compression strength of concrete. According to the same Standards, the mean value of f descends from the characteristic value of the concrete compressive strength f_k by adding a constant. By assuming a normal distribution

Table 6: Comparison between experimental and numerical natural frequencies of the optimized FE models.

	Span No 1				**Span No 5**		
f_n	$f_{\mathbf{exp}}$	$f_{\mathbf{num}}$	$f_{\mathbf{exp}}$-$f_{\mathbf{num}}/f_{\mathbf{exp}}$	f_n	$f_{\mathbf{exp}}$	$f_{\mathbf{num}}$	$f_{\mathbf{exp}}$-$f_{\mathbf{num}}/f_{\mathbf{exp}}$
f_1	8.01	7.34	8.35%	f_1	6.95	6.97	-0.30%
f_2	9.15	8.56	6.42%	f_2	8.44	7.37	12.67%
f_3	14.20	14.48	-1.95%	f_3	13.42	14.88	-10.86%
f_4	-	22.88	-	f_4	22.887	22.65	1.02%
	Span No 2				**Span No 6**		
f_n	$f_{\mathbf{exp}}$	$f_{\mathbf{num}}$	$f_{\mathbf{exp}}$-$f_{\mathbf{num}}/f_{\mathbf{exp}}$	f_n	$f_{\mathbf{exp}}$	$f_{\mathbf{num}}$	$f_{\mathbf{exp}}$-$f_{\mathbf{num}}/f_{\mathbf{exp}}$
f_1	7.17	7.28	-1.55%	f_1	7.15	7.21	-0.84%
f_2	8.68	7.74	10.81%	f_2	8.53	7.63	10.55%
f_3	14.10	15.69	-11.25%	f_3	14.137	15.41	-9.02%
f_4	23.53	22.88	2.76%	f_4	23.73	23.31	1.77%
	Span No 3				**Span No 7**		
f_n	$f_{\mathbf{exp}}$	$f_{\mathbf{num}}$	$f_{\mathbf{exp}}$-$f_{\mathbf{num}}/f_{\mathbf{exp}}$	f_n	$f_{\mathbf{exp}}$	$f_{\mathbf{num}}$	$f_{\mathbf{exp}}$-$f_{\mathbf{num}}/f_{\mathbf{exp}}$
f_1	7.5	7.18	4.27%	f_1	8.27	7.84	5.20%
f_2	8.85	7.56	14.59%	f_2	9.3	8.24	11.40%
f_3	13.45	15.18	-12.84%	f_3	14.6	16.44	-12.60%
f_4	-	23.93		f_4	-	23.45	-
	Span No 4						
f_n	$f_{\mathbf{exp}}$	$f_{\mathbf{num}}$	$f_{\mathbf{exp}}$-$f_{\mathbf{num}}/f_{\mathbf{exp}}$				
f_1	6.98	7.00	-0.31%				
f_2	8.62	7.41	14.02%				
f_3	13.39	14.97	-11.83%				
f_4	23.06	22.61	1.97%				

Table 7: Comparison between experimental and numerical mode shapes in terms of MAC.

	Span No 1				**Span No 5**			
	$f_{1,\mathrm{exp}}$	$f_{2,\mathrm{exp}}$	$f_{3,\mathrm{exp}}$	$f_{4,\mathrm{exp}}$	$f_{1,\mathrm{exp}}$	$f_{2,\mathrm{exp}}$	$f_{3,\mathrm{exp}}$	$f_{4,\mathrm{exp}}$
$f_{1,\mathrm{num}}$	95.68%	0.12%	70.29%		98.95%	0.21%	70.74%	0.04%
$f_{2,\mathrm{num}}$	0.33%	90.79%	0.02%		0.40%	95.47%	0.07%	0.18%
$f_{3,\mathrm{num}}$	99.27%	0.18%	76.15%		97.75%	0.21%	72.19%	0.04%
					0.02%	0.00%	0.01%	94.61%
	Span No 2				**Span No 6**			
$f_{1,\mathrm{num}}$	99.00%	0.12%	72.46%	1.66%	99.27%	0.02%	69.56%	0.52%
$f_{2,\mathrm{num}}$	0.67%	90.79%	0.23%	0.00%	0.42%	95.58%	0.52%	0.17%
$f_{3,\mathrm{num}}$	97.75%	0.11%	73.77%	1.65%	98.10%	0.02%	71.00%	0.52%
$f_{4,\mathrm{num}}$	0.00%	0.00%	0.09%	90.55%	0.01%	0.02%	0.09%	97.03%
	Span No 3				**Span No 7**			
$f_{1,\mathrm{num}}$	99.30%	0.21%	74.10%		99.02%	1.10%	72.76%	
$f_{2,\mathrm{num}}$	0.49%	96.65%	0.07%		0.00%	95.34%	0.68%	
$f_{3,\mathrm{num}}$	97.89%	0.21%	75.97%		97.64%	1.09%	74.16%	
$f_{4,\mathrm{num}}$								
	Span No 4							
$f_{1,\mathrm{num}}$	99.15%	0.24%	76.54%	0.05%				
$f_{2,\mathrm{num}}$	0.09%	95.00%	0.25%	0.04%				
$f_{3,\mathrm{num}}$	97.84%	0.24%	78.07%	0.05%				
$f_{4,\mathrm{num}}$	0.00%	0.05%	0.00%	99.24%				

of the resistance, the standard deviation σ according to [54], is:

$$f = f_k + 8 \rightarrow \sigma = \frac{8}{1.64} = 4.878 \tag{7}$$

In the considered case, the concrete of the girders has a different characteristic value than that of the deck. Tab.4 details the corresponding values and the associated Young's moduli, estimated from Eq.(6). Eq.6 is used to estimate the value of the concrete resistance using Young's modulus, while Eqs.2-3 returned the tolerances of the estimates in terms of variances of Young's modulus (σ_E) and the concrete resistance (σ_f). Tab.8 lists Young's moduli estimated from FE model updating for each of the seven spans and the values of the concrete resistance using Eq.6, with the corresponding uncertainties. There is a substantial difference between Young's moduli of the girder and

Table 8: Estimated parameters. E_b, E_d, σ_{Eb}, and σ_{Ed} are Young's moduli and related variances of the girder and the deck, respectively. f_b, f_d, σ_{fb}, and σ_{fd} are the concrete compressive strength and related variances of the girder and the deck.

Parameters	**Span No 1**	**Span No 2**	**Span No 3**	**Span No 4**	**Span No 5**	**Span No 6**	**Span No 7**
E_{b} [MPa]	44234.63	33754.20	41530.07	34622.50	35227.49	36909.78	48203.66
E_{d} [MPa]	27323.36	29599.20	24647.76	25638.10	24981.85	27088.64	28427.66
$\sigma_{E\mathrm{b}}$ [MPa]	27.41	28.92	23.14	87.38	62.01	66.18	28.21
$\sigma_{E\mathrm{d}}$ [MPa]	55.98	125.07	8.12	128.77	16.80	149.79	35.96
$\sigma_{E\mathrm{b}E\mathrm{d}}$ [MPa]	31.85	60.14	13.71	59.46	32.27	99.56	31.85
f_b [MPa]	81.29	36.12	67.27	38.98	41.06	47.22	105.19
f_d [MPa]	19.16	24.35	14.06	15.83	14.64	18.67	21.58
σ_{fb} [MPa]	0.15	0.09	0.11	0.30	0.22	0.25	0.18
σ_{fd} [MPa]	0.12	0.31	0.01	0.24	0.03	0.31	0.08

the deck, due to the different concrete classes of the girders and the deck. The Young's moduli of the deck approximately span between 24000 and 28000 MPa, while those of the girders between 33000 and 48000. This gap between E reflects a gap between the estimated resistances. The concrete resistance of the deck spans between 15 and 20 MPa, while that of the girders is between 35 and 105 MPa. It appears that the concrete resistance of the deck is lower than the nominal value equal to 30 MPa in Tab.4, while that of the girder is higher than the nominal value equal to 55 MPa. This opposite behaviour probably mirrors the different pouring and curing conditions of the two structural elements. Indeed, the deck was cast in situ, while the girders are made of pre-cast concrete which presents very different porosity, and thus both mechanical and degradation quite differing properties. The variances of the estimates are quite low, due to adoption of a tolerance for the

Table 9: Averaged parameters between the seven spans.

Parameters	Estimated	Reference	Percentage difference
E_b [Mpa]	39211.76	36688.63	6.43%
E_d [Mpa]	26815.22	30588.56	-14.07%
σ_{Eb} [Mpa]	5119.68	194.78	96.20%
σ_{Ed} [Mpa]	1695.72	297.73	82.44%
f_b [Mpa]	59.59	55.00	7.70%
f_d [Mpa]	18.33	30.00	-63.70%
σ_{fb} [Mpa]	26.39	4.88	81.52%
σ_{fd} [Mpa]	24.15	4.88	79.80%

convergence of the objective function equal to 0.01. Tab.9 lists the estimated values of Young's moduli and concrete resistance averaged over the seven spans. Eventually, the concrete resistance of the deck exhibits a significantly lower resistance compared to the reference values in Tab.4, on average equal to 63.70%, while that of the girders showed a slight improvement, on average equal to 7.70%. The reference variances of E and f, estimated from Eq.7 are significantly higher than the tolerances of the estimates, as thoroughly discussed in the next section.

5. Discussion: indirect estimate of the variance of concrete resistance

The above indirect procedure for estimating the concrete resistance from Young's moduli is validated against the values of the concrete resistance evaluated from 3 concrete specimens extracted from each span. Unfortunately, the authors could not extract the specimens from the deck and had to limit the validation to the sole resistance of the girders. Tab.10 compares the values of Young's moduli and resistance of the girders from concrete specimens, labelled with the superscript ^{d}, with those evaluated from the indirect method, labelled with the superscript ^{i}. The authors report the mean value f_b^i and the variance σ_{fb}^i calculated from the three concrete specimens extracted from each girder. Except for span No 7, where the concrete resistance estimated from the FE model updating was far from the actual value, the percentage error of each set of values is approximately between 3% and 23%. Tab.10 proves that an indirect assessment of the concrete resistance based on empirical correlations with Young's moduli and FE model updating using the modal parameters can be a valid alternative to destructive tests. Furthermore, the adoption of the proposed indirect method virtually provides the fundamental advantage of tracking the values of interest over time within a continuous

Table 10: Comparison between the concrete resistance estimated from the FE model updating (indirect) and that estimated from concrete samples (direct).

Span No	Indirect Estimation		Direct Estimation		Percentage difference	
	f_b^i [Mpa]	σ_{fb}^i [Mpa]	f_b^d [Mpa]	σ_{fb}^d [Mpa]	$\frac{f_b^i - f_b^d}{f_b^d}$	$\frac{\sigma_{fb}^i - \sigma_{fb}^d}{\sigma_{fb}^d}$
1	81.29	0.15	67.80	3.20	19.89%	-95.28%
2	36.12	0.09	29.40	1.20	22.85%	-92.26%
3	67.27	0.11	54.40	3.40	23.66%	-96.69%
4	38.98	0.30	42.10	4.50	-7.42%	-93.44%
5	41.06	0.22	38.30	3.10	7.20%	-93.01%
6	47.22	0.25	45.50	2.50	3.79%	-89.84%
7	105.19	0.18	60.20	1.70	74.73%	-89.14%

monitoring system. Conversely, the extraction of concrete samples is limited since it cannot compromise the bridge's structural capacity. Additionally, the concrete resistances assessed from the indirect method are global representatives of the structural performances. The percentage differences of the two variances are approximately 100%. Thus, the reference variance is far higher than that obtained by propagating the variance of the objective function. Actually, it is worth noting that the two variances are not directly comparable because they derive from two different sources of uncertainties. First, the variance determined from the FE model updating expresses a modeling error. At the same time, the one from concrete samples represents the spatial variability of the concrete resistance, which cannot be estimated with a FE model where Young's modulus is constant along the girder. The Young's modulus of concrete is not a homogenized parameter, uniform inside the structure, but it can vary from point to point. Specifically, concrete exhibits significant scatter in its mechanical properties. The issue of damage localization entails developing a refined FE model, where the structure is divided into multiple sections with a distinct Young's modulus. However, this approach is computationally expensive and quite advanced for engineering practice. If Young's modulus is assumed uniform inside the structure, estimating its intrinsic scatter due to spatial variability is impracticable. In conclusion, in concrete constructions, capacity estimation generally requires assessing compressive strength from extracted samples. Furthermore, in addition to spatial variability, we must not forget that epistemic uncertainty and aleatory variability may contribute to the variability of the measured and estimated parameters. However, this research proved that FE model updating of Young's moduli using the experimental modal parameters and suitable correlations between Young's moduli and concrete resistance could be a valid indirect method for

assessing concrete resistance. In the perspective of continuous dynamic monitoring, this approach can continuously track the mechanical parameters for potential nearly real-time assessment of the structural capacity. However, estimating the variance of the concrete strength inside the structure cannot be obtained from a FE model with constant values of Young's moduli. Therefore, the goal of FE model updating is to assess the mechanical parameters. At the same time, their uncertainty due to spatial variability can be assessed if there are no destructive tests.

6. Concluding remarks

The paper addresses the reliability in estimating the compressive strength of concrete using acknowledged correlations between the concrete resistance and Young's moduli, the latter estimated from FE model updating using the experimental modal parameters. The compressive resistance estimated from this indirect method is compared to the values obtained from the experimental tests of concrete specimens.

The authors carried out the experimental investigation on a seven-spans prestressed-concrete bridge in Corvara (Italy). The Operational Modal Analysis led to the experimental modal parameters and the consequent model updating of Young's moduli of the deck and the girders based on the Particle Swarm Optimization and Differential Evolution algorithms. The two algorithms returned almost coincident values, proving that the optimization was well-posed.

The estimated resistance of the deck and the girders differed from the reference values assumed in the design. After almost 30 years of life, the deck's concrete resistance exhibited an average 60% decrement, while the girders' resistance had an approximate 7% increment. The dissimilar long-term behaviour of the deck and the girders, confirmed by the experimental tests, mirrors the different concrete curing and pouring conditions at the time of construction.

The outcomes of the proposed indirect method for estimating the compressive strength of concrete are entirely confirmed by the resistances of the concrete specimens extracted from each span. The percentage error between the compressive strengths obtained from the two methods is approximately 20%. The indirect estimates are generally associated with an overestimation of Young's moduli. This fact may depend on the nonlinear behaviour of concrete and the plausible higher stiffness at lower vibration levels, typical of an

operational condition without the transit of vehicles.
The variances from the indirect method are much higher than those obtained from the concrete samples extracted from the bridge. The two variances refer to at least two different sources of uncertainties and may not be directly compared. The variance from concrete specimens expresses the spatial scatter of the mechanical properties of concrete inside the structure. Even if the sensor placement considers intrinsically the spatial variability of the recorded operational response, the simplified global FE model for each span only considers a variation among the spans and not along the same span. The variance derived from the FE optimization refers to the model error and expresses the tolerances of the estimates. In conclusion, the combined FE model updating with modal data and empirical correlation between Young's modulus and concrete may represent a valid alternative to destructive tests, especially if continuous monitoring of the concrete state is required. In future researches, the authors will aim at developing multivariate probabilistic capacity models by integrating Operational Modal Analysis and FE model optimization.

7. Data availability statement

The Matlab code that supports the findings of this study is available from the corresponding author upon reasonable request.

8. Declaration of Competing Interest

The authors declare that they have no known competing financial interests or personal relationships that could have appeared to influence the work reported in this paper.

Appendix A. Experimental mode shapes

Table A.11: Experimental Mode Shapes of Span No 1

Span No 1							
$\Phi_{1,v}$	$\Phi_{1,h}$	$\Phi_{2,h}$	$\Phi_{2,v}$	$\Phi_{3,h}$	$\Phi_{3,v}$	$\Phi_{4,v}$	$\Phi_{4,h}$
0.097	4E-04	-0.1	-0.027	0.115	0.129	-	-
0.731	0.019	-0.714	0.023	0.803	0.484	-	-
0.973	0.01	-0.913	0.049	1	0.635	-	-
0.626	0.009	-0.577	0.027	0.665	0.435	-	-
0.044	0.001	-0.033	-0.006	0.065	0.151	-	-
0.017	0.001	0.031	-0.012	0.015	-0.004	-	-
0.646	-0.02	0.63	0.023	0.44	-0.286	-	-
1	-0.037	1	0.042	0.622	-0.529	-	-
0.745	-0.026	0.761	0.032	0.538	-0.415	-	-
0.072	-0.019	0.079	-0.024	0.104	-0.091	-	-

Table A.12: Experimental Mode Shapes of Span No 2

Span No 2							
$\Phi_{1,v}$	$\Phi_{1,h}$	$\Phi_{2,h}$	$\Phi_{2,v}$	$\Phi_{3,h}$	$\Phi_{3,v}$	$\Phi_{4,v}$	$\Phi_{4,h}$
0.042	0.015	-0.044	0.01	0.074	0.078	-0.07	-0.052
0.559	0.015	-0.641	0.042	0.644	0.352	-0.424	-0.068
0.803	0.025	-0.929	0.056	0.899	0.5	-0.139	-0.035
0.565	0.038	-0.64	0.048	0.654	0.335	0.416	0.016
0.017	0.046	-0.01	0.031	0.017	0.018	0.052	0.04
0.012	0.041	0.024	0.032	0.045	-0.048	0.133	0.019
0.683	0.035	0.681	0.046	0.76	-0.41	1	0.014
1	0.023	1	0.047	1	-0.632	-0.227	-0.047
0.697	0.014	0.678	0.035	0.634	-0.443	-0.971	-0.056
0.032	-0.011	0.051	0.004	0.137	-0.124	-0.18	-0.005

Table A.13: Experimental Mode Shapes of Span No 3

Span No 3							
$\Phi_{1,v}$	$\Phi_{1,h}$	$\Phi_{2,h}$	$\Phi_{2,v}$	$\Phi_{3,h}$	$\Phi_{3,v}$	$\Phi_{4,v}$	$\Phi_{4,h}$
-0.006	-0.005	0.002	0.002	0.011	-0.035	-	-
0.638	-0.005	-0.456	-0.024	0.733	0.386	-	-
1	-0.014	-0.707	-0.052	0.996	0.606	-	-
0.731	-0.008	-0.516	-0.105	0.757	0.398	-	-
0.02	0.003	-0.037	-0.158	0.09	-0.005	-	-
0.011	0.008	0.034	-0.151	0.024	-0.086	-	-
0.592	0.004	0.678	-0.1	0.685	-0.385	-	-
0.874	0.005	1	-0.051	1	-0.558	-	-
0.58	0.008	0.647	-0.021	0.64	-0.393	-	-
-0.015	0.005	-0.011	-0.004	0.015	-0.098	-	-

Table A.14: Experimental Mode Shapes of Span No 4

Span No 4							
$\Phi_{1,v}$	$\Phi_{1,h}$	$\Phi_{2,h}$	$\Phi_{2,v}$	$\Phi_{3,h}$	$\Phi_{3,v}$	$\Phi_{4,v}$	$\Phi_{4,h}$
-0.062	0.049	0.027	-0.008	0.003	0.033	0.313	-0.136
0.591	0.036	-0.584	0.024	0.684	0.337	1	-0.11
0.93	0.032	-0.908	0.033	1	0.513	0.202	-0.017
0.652	0.029	-0.624	0.01	0.672	0.369	-0.794	0.014
0.013	0.026	-0.01	-0.024	0.008	0.075	-0.101	0.05
-0.019	0.037	-0.01	-0.022	-0.014	0.015	-0.107	0.013
0.7	0.045	0.688	0.006	0.594	-0.326	-0.662	-0.015
1	0.05	1	0.021	0.906	-0.505	0.053	-0.01
0.658	0.054	0.646	0.021	0.601	-0.33	0.737	-0.043
-0.017	0.045	-0.004	-0.011	0.001	-0.062	0.149	-0.091

Table A.15: Experimental Mode Shapes of Span No 5

Span No 5							
$\Phi_{1,v}$	$\Phi_{1,h}$	$\Phi_{2,h}$	$\Phi_{2,v}$	$\Phi_{3,h}$	$\Phi_{3,v}$	$\Phi_{4,v}$	$\Phi_{4,h}$
0.025	0.07	0.025	0.037	0.001	0.103	-0.099	0.019
0.61	0.038	0.704	-0.004	0.721	0.476	-0.955	0.021
0.885	0.006	1	-0.02	1	0.67	0.087	-0.017
0.593	-0.025	0.657	-0.009	0.683	0.427	1	-0.069
-0.005	-0.056	0.006	0.007	0.011	0.044	0.042	-0.029
0.03	-0.044	-0.028	0.007	0.035	-0.076	0.036	0.006
0.678	-0.024	-0.601	-0.01	0.655	-0.366	0.621	-0.006
1	0.003	-0.91	-0.013	0.978	-0.58	-0.013	-0.04
0.71	0.034	-0.643	6E-04	0.657	-0.387	-0.673	-0.042
0.025	0.065	-0.033	0.031	-0.006	-0.056	-0.103	-0.02

Table A.16: Experimental Mode Shapes of Span No 6

Span No 6							
$\Phi_{1,v}$	$\Phi_{1,h}$	$\Phi_{2,h}$	$\Phi_{2,v}$	$\Phi_{3,h}$	$\Phi_{3,v}$	$\Phi_{4,v}$	$\Phi_{4,h}$
0.024	0.007	-0.03	-0.011	0.052	0.081	-0.106	0.017
0.592	8E-04	-0.632	0.005	0.567	0.39	-0.964	0.088
0.893	-0.021	-0.986	0.023	0.826	0.542	0.022	0.081
0.592	-0.028	-0.632	-0.002	0.567	0.364	0.964	0.037
0.049	-0.043	-0.047	-0.029	0.036	0.059	0.117	-0.036
0.035	-0.036	0.032	-0.036	0.057	-0.078	0.067	0.012
0.696	-0.026	0.688	5E-04	0.714	-0.397	1	0.092
1	-0.015	1	0.015	1	-0.616	0.12	0.101
0.664	-0.004	0.636	0.008	0.586	-0.378	-0.815	0.04
0.027	0.005	0.022	-0.013	0.027	-0.058	-0.08	0.01

Table A.17: Experimental Mode Shapes of Span No 7

Span No 7							
$\Phi_{1,v}$	$\Phi_{1,h}$	$\Phi_{2,h}$	$\Phi_{2,v}$	$\Phi_{3,h}$	$\Phi_{3,v}$	$\Phi_{4,v}$	$\Phi_{4,h}$
0.02	0.061	0.054	0.118	0.056	0.035	-	-
0.692	0.066	0.691	0.095	0.565	0.334	-	-
0.95	0.036	1	0.042	0.836	0.486	-	-
0.692	0.015	0.691	0.024	0.565	0.33	-	-
0.092	0.004	0.086	0.024	0.067	0.062	-	-
0.084	0.003	-0.064	0.017	0.117	-0.068	-	-
0.66	0.023	-0.563	0.006	0.676	-0.376	-	-
1	0.037	-0.82	0.024	1	-0.573	-	-
0.707	0.053	-0.536	0.073	0.674	-0.396	-	-
-0.002	0.064	-0.05	0.118	0.051	-0.09	-	-

References

[1] P. Brinckerhoff, A review of bridge assessment failures on the motorway and trunk road network, Highways Agency Contract 2 (2003) 419.

[2] L. Deng, W. Wang, Y. Yu, State-of-the-art review on the causes and mechanisms of bridge collapse, Journal of Performance of Constructed Facilities 30 (2) (2016) 04015005.

[3] C. Rainieri, G. Fabbrocino, Operational modal analysis of civil engineering structures, Springer, New York 142 (2014) 143.

[4] M. Abdulkarem, K. Samsudin, F. Z. Rokhani, M. F. A Rasid, Wireless sensor network for structural health monitoring: A contemporary review of technologies, challenges, and future direction, Structural Health Monitoring 19 (3) (2020) 693–735.

[5] N. G. Pnevmatikos, G. D. Hatzigeorgiou, Damage detection of framed structures subjected to earthquake excitation using discrete wavelet analysis, Bulletin of Earthquake Engineering 15 (2017) 227–248. doi:https://doi.org/10.1007/s10518-016-9962-z.

[6] N. Pnevmatikos, F. Konstandakopoulou, B. Blachowski, G. Papavasileiou, P. Broukos, Multifractal analysis and wavelet leaders for structural damage detection of structures subjected to earthquake excitation, Soil Dynamics and Earthquake Engineering 139 (2020) 106328. doi:https://doi.org/10.1016/j.soildyn.2020.106328.
URL `https://www.sciencedirect.com/science/article/pii/S0267726120303791`

[7] Z. Wang, X. C. Man, R. D. Finch, B. H. Jansen, The dynamic behavior and vibration monitoring of reinforced concrete beams, Journal of testing and evaluation 26 (5) (1998) 405–419.

[8] W.-X. Ren, G. De Roeck, Structural damage identification using modal data. i: Simulation verification, Journal of Structural Engineering 128 (1) (2002) 87–95.

[9] J.-M. Ndambi, J. Vantomme, K. Harri, Damage assessment in reinforced concrete beams using eigenfrequencies and mode shape derivatives, Engineering structures 24 (4) (2002) 501–515.

[10] Y. Yan, L. Cheng, Z. Wu, L. Yam, Development in vibration-based structural damage detection technique, Mechanical systems and signal processing 21 (5) (2007) 2198–2211.

[11] P. F. Giordano, S. Quqa, M. P. Limongelli, Statistical approach for vibration-based damage localization in civil infrastructures using smart sensor networks, Infrastructures 6 (2) (2021) 22.

[12] S. Quqa, L. Landi, P. P. Diotallevi, Modal assurance distribution of multivariate signals for modal identification of time-varying dynamic systems, Mechanical Systems and Signal Processing 148 (2021) 107136.

[13] A. Aloisio, L. Di Battista, R. Alaggio, M. Fragiacomo, Sensitivity analysis of subspace-based damage indicators under changes in ambient excitation covariance, severity and location of damage, Engineering Structures 208 (2020) 110235.

[14] G. Li, Y. Zhao, S.-S. Pang, Y. Li, Effective young's modulus estimation of concrete, Cement and Concrete Research 29 (9) (1999) 1455–1462.

[15] A. Aloisio, D. P. Pasca, R. Alaggio, M. Fragiacomo, Bayesian estimate of the elastic modulus of concrete box girders from dynamic identification: a statistical framework for the a24 motorway in italy, Structure and Infrastructure Engineering (2020) 1–13.

[16] D. Hobbs, The dependence of the bulk modulus, young's modulus, creep, shrinkage and thermal expansion of concrete upon aggregate volume concentration, Matériaux et construction 4 (2) (1971) 107–114.

[17] M. Alves, J. Yu, N. Jones, On the elastic modulus degradation in continuum damage mechanics, Computers & Structures 76 (6) (2000) 703–712.

[18] Y. Yu, T. N. Nguyen, J. Li, L. F. Sanchez, A. Nguyen, Predicting elastic modulus degradation of alkali silica reaction affected concrete using soft computing techniques: A comparative study, Construction and Building Materials 274 (2021) 122024.

[19] I. Tien, A. Der Kiureghian, Algorithms for bayesian network modeling and reliability assessment of infrastructure systems, Reliability Engineering & System Safety 156 (2016) 134–147.

[20] M. Rashid, M. Mansur, P. Paramasivam, Correlations between mechanical properties of high-strength concrete, Journal of materials in civil engineering 14 (3) (2002) 230–238.

[21] I. Shkolnik, Effect of nonlinear response of concrete on its elastic modulus and strength, Cement and Concrete Composites 27 (7-8) (2005) 747–757.

[22] M. Azenha, L. F. Ramos, R. Aguilar, J. L. Granja, Continuous monitoring of concrete e-modulus since casting based on modal identification: A case study for in situ application, Cement and Concrete Composites 34 (7) (2012) 881–890.

[23] M. Ohtsu, H. Watanabe, Quantitative damage estimation of concrete by acoustic emission, Construction and Building Materials 15 (5-6) (2001) 217–224.

[24] Y. Akkaya, T. Voigt, K. Subramaniam, S. P. Shah, Nondestructive measurement of concrete strength gain by an ultrasonic wave reflection method, Materials and structures 36 (8) (2003) 507–514.

[25] ASTM-C215, Standard test method for fundamental transverse, longitudinal, and torsional resonant frequencies of concrete specimens., ASTM International (2008).

[26] D. A. für Stahlbeton, Prüfung von beton, empfehlungen und hinweise als ergänzung zu din 1048, Bundesanstalt für Straßenwesen (BASt) (1991).

[27] M. Azenha, L. F. Ramos, R. Aguilar, J. L. Granja, Continuous monitoring of concrete e-modulus since casting based on modal identification: A case study for in situ application, Cement and Concrete Composites 34 (7) (2012) 881–890.

[28] A. Teughels, G. De Roeck, Structural damage identification of the highway bridge z24 by fe model updating, Journal of Sound and Vibration 278 (3) (2004) 589–610.

[29] A. M. Neville, et al., Properties of concrete, Vol. 4, Longman London, 1995.

[30] J. E. Mottershead, M. Friswell, Model updating in structural dynamics: a survey, Journal of sound and vibration 167 (2) (1993) 347–375.

[31] A. Der Kiureghian, O. Ditlevsen, Aleatory or epistemic? does it matter?, Structural safety 31 (2) (2009) 105–112.

[32] C. Soize, Generalized probabilistic approach of uncertainties in computational dynamics using random matrices and polynomial chaos decompositions, International Journal for Numerical Methods in Engineering 81 (8) (2010) 939–970.

[33] C. Soize, Stochastic modeling of uncertainties in computational structural dynamics—recent theoretical advances, Journal of Sound and Vibration 332 (10) (2013) 2379–2395.

[34] M. C. Kennedy, A. O'Hagan, Bayesian calibration of computer models, Journal of the Royal Statistical Society: Series B (Statistical Methodology) 63 (3) (2001) 425–464.

[35] W. E. Walker, P. Harremoës, J. Rotmans, J. P. Van Der Sluijs, M. B. Van Asselt, P. Janssen, M. P. Krayer von Krauss, Defining uncertainty: a conceptual basis for uncertainty management in model-based decision support, Integrated assessment 4 (1) (2003) 5–17.

[36] E. Simoen, G. De Roeck, G. Lombaert, Dealing with uncertainty in model updating for damage assessment: A review, Mechanical Systems and Signal Processing 56 (2015) 123–149.

[37] M. A. Wahab, G. De Roeck, B. Peeters, Parameterization of damage in reinforced concrete structures using model updating, Journal of Sound and Vibration 228 (4) (1999) 717–730.

[38] M. Friswell, J. E. Mottershead, Finite element model updating in structural dynamics, Vol. 38, Springer Science & Business Media, 2013.

[39] K. Jurowski, S. Grzeszczyk, The influence of concrete composition on young's modulus, Procedia Engineering 108 (2015) 584–591.

[40] E. Reynders, System identification methods for (operational) modal analysis: review and comparison, Archives of Computational Methods in Engineering 19 (1) (2012) 51–124.

[41] S. Pereira, E. Reynders, F. Magalhães, Á. Cunha, J. P. Gomes, The role of modal parameters uncertainty estimation in automated modal identification, modal tracking and data normalization, Engineering Structures 224 (2020) 111208.

[42] R. Alaggio, A. Aloisio, E. Antonacci, R. Cirella, Two-years static and dynamic monitoring of the santa maria di collemaggio basilica, Construction and Building Materials 268 (2021) 121069.

[43] R. Brincker, L. Zhang, P. Andersen, Modal identification of output-only systems using frequency domain decomposition, Smart materials and structures 10 (3) (2001) 441.

[44] B. Peeters, G. De Roeck, Reference-based stochastic subspace identification for output-only modal analysis, Mechanical systems and signal processing 13 (6) (1999) 855–878.

[45] A. Aloisio, R. Alaggio, M. Fragiacomo, Dynamic identification and model updating of full-scale concrete box girders based on the experimental torsional response, Construction and Building Materials 264 (2020) 120146.

[46] E. Sapountzakis, J. Katsikadelis, Elastic deformation of ribbed plates under static, transverse and inplane loading, Computers & Structures 74 (5) (2000) 571–581.

[47] C. Rainieri, G. Fabbrocino, E. Cosenza, Some remarks on experimental estimation of damping for seismic design of civil constructions, Shock and Vibration 17 (4, 5) (2010) 383–395.

[48] R. J. Allemang, D. L. Brown, A correlation coefficient for modal vector analysis, in: Proceedings of the 1st international modal analysis conference, Vol. 1, SEM Orlando, 1982, pp. 110–116.

[49] D. P. Pasca, A. Aloisio, M. Fragiacomo, R. Tomasi, Dynamic characterization of timber floor subassemblies: Sensitivity analysis and modeling issues, Journal of Structural Engineering 147 (12) (2021) 05021008.

[50] M. Saisana, A. Saltelli, S. Tarantola, Uncertainty and sensitivity analysis techniques as tools for the quality assessment of composite indicators, Journal of the Royal Statistical Society: Series A (Statistics in Society) 168 (2) (2005) 307–323.

[51] R. Storn, K. Price, Differential evolution–a simple and efficient heuristic for global optimization over continuous spaces, Journal of global optimization 11 (4) (1997) 341–359.

[52] R. Eberhart, J. Kennedy, Particle swarm optimization, in: Proceedings of the IEEE international conference on neural networks, Vol. 4, Citeseer, 1995, pp. 1942–1948.

[53] A. Teughels, G. De Roeck, J. A. Suykens, Global optimization by coupled local minimizers and its application to fe model updating, Computers & structures 81 (24-25) (2003) 2337–2351.

[54] L. G. NTC, Norme tecniche per le costruzioni, Italian technical norms for constructions (2018).